Role of parametric resonances in global chaos

D. Jeon, M. Bai, C. M. Chu, X. Kang, S. Y. Lee, A. Riabko, and X. Zhao
Department of Physics, Indiana University, Bloomington, Indiana 47405
(Received 18 April 1996)

The quasi-isochronous (QI) dynamical system, in the presence of synchrotron radiation damping and rf phase modulation, exhibits a sequence of period-2 bifurcations en route towards global chaos (instability) in a region of modulation tune. The critical modulation amplitude for the onset of the global chaos shows a cusp as a function of the modulation tune. This cusp is shown to arise from the transition from the 2:1 to the 1:1 parametric resonances. We have also studied the effect of the rf voltage modulation on the QI dynamical system and found that the tolerance of the rf voltage modulation is much larger than that of the rf phase modulation. [S1063-651X(96)07509-5]

PACS number(s): 29.20.Dh, 03.20.+i, 05.45.+b

I. INTRODUCTION

Very short electron bunches, e.g., submillimeter in bunch length, can enhance applications such as time resolved experiments, next generation light sources, coherent synchrotron radiations, and damping rings for the next linear colliders. A possible method to produce short bunches is to reduce the phase slip factor, or the momentum compaction factor for electron storage rings. Because of its potential benefit, the physics of particle dynamics in low α_c lattices is important [1–8].

In our earlier paper [1], we transformed the quasi-isochronous (QI) synchrotron Hamiltonian into a universal Weierstrass equation, where particle motion could be described by the Weierstrass $\wp$ function or the Jacobian elliptic function [9,10]. We showed that the QI dynamical system exhibited chaos at a relatively weak rf phase modulation. Due to the synchrotron radiation damping, stable fixed points (SFPs) of parametric resonances become attractors. As the amplitude of the applied phase modulation increases, the system exhibits a sequence of period-2 bifurcations en route towards global chaos in a region of the modulation tune. The sequence of period-2 bifurcations has been attributed to parametric resonances of the Hamiltonian system. When the critical phase modulation amplitude is plotted as a function of the modulation tune, a cusp appears. The question is, what causes the cusp in the stability of this dynamical system? Furthermore, what is the effect of the rf voltage modulation?

This paper studies the role of parametric resonances on the stability of the QI dynamical system. Section II studies the effect of parametric resonances due to the rf phase modulation on the stability of the dynamical system. Section III studies the effect of the rf voltage modulation on particle motion. The conclusion is given in Sec. IV.

II. THE STABILITY OF QI SYSTEM WITH rf PHASE MODULATION

The equation of motion for the rf phase coordinate ϕ of a particle in a synchrotron is given by

$$\dot{\phi}=h\eta\delta, \tag{1}$$

where h is the harmonic number, $\delta=\Delta p/p$ is the fractional momentum deviation from the synchronous particle, the overdot is the derivative with respect to the orbiting angle $\theta=s/R_0$, and η is the phase slip factor given by

$$\eta=\eta_0+\eta_1\delta+\cdots, \tag{2}$$

where η_0 and η_1 are the first order and the second order phase slip factor. In many realistic storage rings, the truncation of the phase slip factor at the η_1 term is a good approximation. Similarly, the equation of motion for the fractional off-momentum deviation is given by

$$\dot{\delta}=\frac{eV_0}{2\pi\beta^2E_0}(\sin\phi-\sin\phi_s), \tag{3}$$

where V_0 and ϕ_s are the rf voltage and the synchronous phase angle, and βc and E_0 are the velocity and the energy of the beam.

Using $t=\nu_s\theta$ as the time variable, where $\nu_s=\sqrt{he V_0|\eta_0\cos\phi_s|/2\pi\beta^2E_0}$ is the small amplitude synchrotron tune, and using (x,p) as conjugate phase space coordinates, where

$$x=-\frac{\eta_1}{\eta_0}\frac{\Delta p}{p_0}, \quad p=\frac{dx}{dt}, \tag{4}$$

the synchrotron Hamiltonian for particle motion in QI storage rings is given by [1]

$$H_0=\frac{1}{2}p^2+\frac{1}{2}x^2-\frac{1}{3}x^3. \tag{5}$$

Since the universal Hamiltonian is autonomous, the ''energy'' E is a constant of motion. For particles inside the bucket, $E\in[0,\frac{1}{6}]$.

The equation of motion in the QI Hamiltonian with energy E is given by the standard Weierstrass equation:

$$\left(\frac{d\wp(u)}{du}\right)^2=4(\wp-e_1)(\wp-e_2)(\wp-e_3), \tag{6}$$

where $u=(1/\sqrt{6})\,t$, $\wp=x$, and turning points are given by $e_1=\frac{1}{2}+\cos(\xi)$, $e_2=\frac{1}{2}+\cos(\xi-120°)$, $e_3=\frac{1}{2}+\cos(\xi+120°)$,

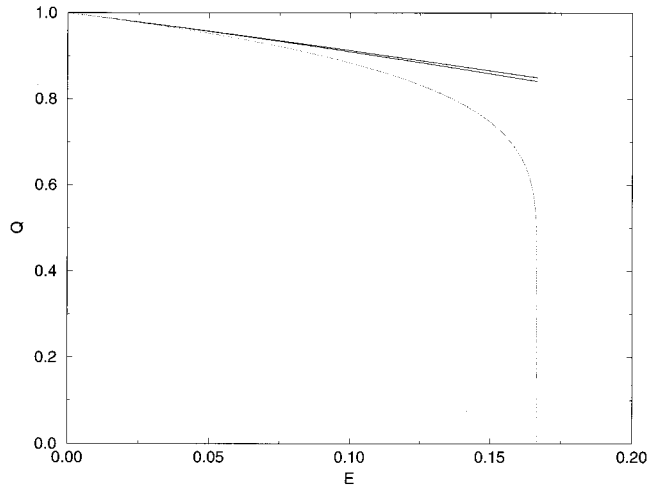

FIG. 1. $Q(E)$ vs E. Because of the sharp drop in synchrotron tune, many parametric resonances overlap with one another near the separatrix trajectory leading to chaos. The upper and the lower ''straight lines'' are, respectively, tunes obtained from the first order and the second canonical order perturbation expansions.

with $\xi=\frac{1}{3}\arccos(1-12E)$. The Weierstrass elliptic $\wp$ function is a single valued doubly periodic function of a single complex variable. For a particle inside the separatrix, the discriminant $\Delta=648E(1-6E)$ is positive, and the Weierstrass $\wp$ function can be expressed in terms of the Jacobian elliptic function [10]

$$x(t)=e_3+(e_2-e_3)\mathrm{sn}^2\left(\sqrt{\frac{e_1-e_3}{6}}t\middle|m\right), \tag{7}$$

$$m=\frac{e_2-e_3}{e_1-e_3}=\frac{\sin\xi}{\sin(\xi+60°)}. \tag{8}$$

The separatrix orbit, which corresponds to $m=1$, is given by

$$x_{sx}(t)=1-\frac{3}{\cosh t+1},\quad p_{sx}(t)=\frac{3\ \sinh t}{(\cosh t+1)^2}. \tag{9}$$

The tune of the QI Hamiltonian is given by

$$Q(E)=\frac{\pi[\sqrt{3}\ \sin(\xi+60°)]^{1/2}}{\sqrt{6}K(m)}, \tag{10}$$

which is shown in Fig. 1 as a function of the energy E. We note particularly that the synchrotron tune decreases to zero very sharply near the separatrix. Because of the sharp decrease in synchrotron tune, time dependent perturbation will cause overlapping parametric resonances and chaos near the separatrix [11–13]. The action of a torus is given by

$$J=\frac{1}{2\pi}\oint p\,dx$$
$$=\frac{1}{8}\sqrt{\frac{2}{3}}(e_2-e_3)^2(e_1-e_3)^{1/2}F\left(\frac{3}{2},-\frac{1}{2};3;m\right), \tag{11}$$

where F is the hypergeometric function [10]. Using the generating function

$$F_2(x,J)=\int_{e_3}^{x}p\,dx, \tag{12}$$

the angle variable is given by $\psi=\partial F_2/\partial J=Qt$.

Due to the synchrotron radiation damping, the equation of motion for QI storage rings is given by

$$x''+Ax'+x-x^2=0, \tag{13}$$

where the effective damping coefficient is given by

$$A=\frac{\lambda}{\nu_s}=\frac{U_0J_E}{2\pi E_0\nu_s}, \tag{14}$$

with the damping decrement λ, the energy loss per revolution U_0, and the damping partition number J_E. In QI storage rings, the effective damping coefficient is enhanced by the corresponding decrease in the synchrotron tune, i.e., $A\sim|\eta_0|^{-1/2}$, where the value of A can vary from 0 to 0.5.

In any realistic dynamical system, time dependent perturbation is unavoidable. In the presence of the rf phase noise, the Hamiltonian in the normalized phase space coordinates is given by

$$H=\frac{p^2}{2}+\frac{1}{2}x^2-\frac{1}{3}x^3+\omega_mBx\ \cos\omega_mt, \tag{15}$$

where $\omega_m=\nu_m/\nu_s$ is the normalized modulation tune, and a and ν_m are, respectively, the rf phase modulation amplitude and the modulation tune in the original accelerator coordinate system. Note that the effective modulation amplitude given by

$$B=\frac{\eta_1a}{\eta_0\nu_s} \tag{16}$$

is greatly enhanced for QI storage rings, i.e., $B\sim|\eta_1|/|\eta_0|^{3/2}$. Including the damping force, the equation of motion becomes

$$x''+Ax'+x-x^2=-\omega_mB\ \cos\omega_mt. \tag{17}$$

A. The width of stochastic layer near the separatrix

In many dynamical systems, e.g., the Duffing oscillator, particle motion is bounded, thus global chaos plays little role in the stability of the dynamical system. On the other hand, the stability region for the QI Hamiltonian system is limited to a finite region of phase space. Existence of global chaos can enhance the probability of unbounded particle motion. This section examines the condition for the stability of the QI dynamical system.

First we examine the effect of rf phase modulation in the absence of friction, where we expand the phase space coordinate in action-angle variables [1]:

$$x=g_0+\sum_{n=1}^{\infty}g_n\cos n\psi, \tag{18}$$

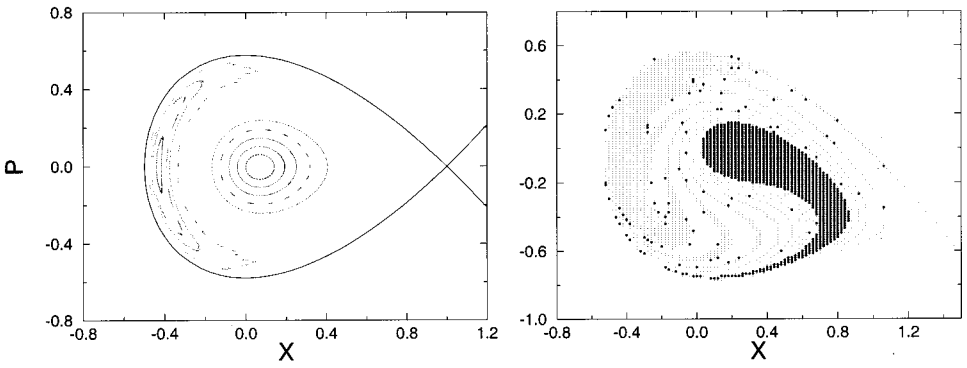

FIG. 2. The Poincaré surface of section for $\omega_m = 0.86$ with parameters $B = 0.02$ is shown in the left plot. With $A = 0$, the dynamical system can tolerate only a small modulation amplitude B. The right plot shows the basin of attraction for the corresponding SFPs with parameters $\omega_m = 0.86, B = 0.06$, and the damping parameter $A = 0.05$. Lightly shaded area damps to the outer attractor and darker shaded area converges to the inner attractor. All particles in the white space are unstable.

$$p = -Q\sum_{n=1}^{\infty} n g_n \sin n\psi, \tag{19}$$

where

$$g_0 = e_3 + (e_1 - e_3)\frac{K(m) - E(m)}{K(m)},$$

$$g_n = (e_1 - e_3)\frac{2\pi^2}{K^2(m)}\frac{(-1)^n n q^n}{1 - q^{2n}}, \tag{20}$$

with $q = e^{-\pi K'/K}$. Here K and E are complete elliptic integrals of the first and the second kind, respectively.

The Hamiltonian of Eq. (15) with rf phase modulation can be expressed as

$$H = H_0(J) + \frac{1}{2}\sum_{n=1}^{\infty} \omega_m B g_n(J)[\cos(n\psi - \omega_m t) + \cos(n\psi + \omega_m t)]. \tag{21}$$

When the modulation frequency is near a synchrotron harmonic, e.g., $\omega_m \approx nQ(J)$, Hamiltonian tori will be perturbed coherently by the resonance term due to the stationary phase condition. Transforming the Hamiltonian into the resonance rotating frame with the generating function $F_2 = [\psi - (\omega_m/n)t]J_1$, the Hamiltonian in the resonance rotating frame becomes

$$H_{n:1} = H_0(J_1) - \frac{\omega_m}{n}J_1 + h_n(J_1)\cos(n\psi_1) + \Delta H_{n:1}(t), \tag{22}$$

where the remaining time dependent (incoherent) terms are lumped into $\Delta H_{n:1}(t)$. Because the effective resonance strength $h_n(J) = \frac{1}{2}\omega_m B g_n(J)$ is proportional to g_n, the expansion coefficients of the phase space coordinate in Eq. (18) are also called resonance strength functions. The stable and unstable fixed points (SFP and UFP) for the time averaged resonance Hamiltonian of Eq. (22) are given by

$$\sin n\psi_{1\mathrm{FP}} = 0, \quad \omega_m = nQ(J_{1\mathrm{FP}}) \pm n\left.\frac{dh_n}{dJ}\right|_{J=J_{1\mathrm{FP}}}. \tag{23}$$

The left plot of Fig. 2 shows an example of the Poincaré surfaces of section with parameters $(B, \omega_m) = (0.02, 0.86)$, where SFPs of two resonance islands in the phase space can be obtained from Eq. (23) with $n = 1$. Without phase space damping, the tolerable value of B is small.

These two resonance islands rotate around the center of the bucket with tune $Q(J_{\mathrm{FP}})$. The sharp drop of synchrotron tune shown in Fig. 1 causes many parametric resonances to overlap with one another near the separatrix orbit. This gives rise to the local instability in a region of phase space between two resonance islands shown in Fig. 2, where the stable region is limited to phase space areas around two SFPs.

The breakdown of Hamiltonian tori near the separatrix is determined by the resonance condition given by

$$\omega_m \approx \frac{n}{\ell}Q(E_{n:\ell}) \quad (n, \ell \text{ are integers}), \tag{24}$$

which is satisfied for all high order parametric resonances with $n/\ell \geq \omega_m$. Since the $Q(E)$ of the QI Hamiltonian drops sharply near the separatrix, all parametric resonances $n{:}\ell$ of Eq. (24) overlap near the separatrix. The width of the stochastic layer is determined by the overlapping region of these parametric resonances. The stochastic layer width is usually characterized by the whisker map introduced by Chirikov [15] to be discussed as follows.

We consider the Hamiltonian of Eq. (15). The energy change rate due to the time dependent perturbation is given by

$$\frac{dH_0}{dt} = \frac{\partial H_0}{\partial t} + [H_0, H] = -\omega_m B p \cos\omega_m t. \tag{25}$$

Using the separatrix orbit of Eq. (9), the energy change in one complete orbit is given by

$$\Delta E = -\omega_m B\int_{-\infty}^{\infty} p_{sx}(t - t_0)\cos\omega_m t\, dt = \frac{6\pi\omega_m^3 B}{\sinh\pi\omega_m}\sin\phi, \tag{26}$$

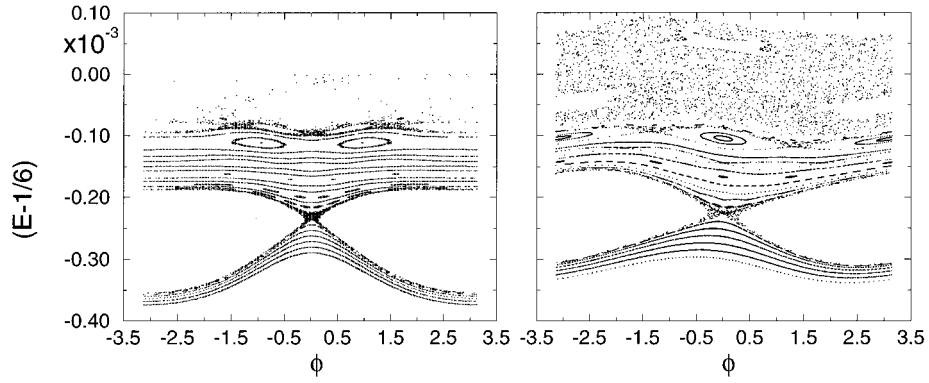

FIG. 3. The whisker map for $B=0.003, \omega_m=4$ is shown in the right plot. The corresponding phase space map obtained from numerical simulations of Eq. (17) is shown in the left plot.

where $\phi=\omega_m t_0$. The revolution period near the separatrix is given by

$$T(E)=2\sqrt{\frac{6}{e_1-e_3}}K(m)\approx 4\ \ln\frac{4}{\sqrt{1-m}}\approx\ln\left(\frac{144}{|\frac{1}{6}-E|}\right). \tag{27}$$

Thus the whisker map is given by

$$E_{n+1}=E_n+\frac{6\pi\omega_m^3 B}{\sinh\pi\omega_m}\sin\phi_n, \tag{28}$$

$$\phi_{n+1}=\phi_n+\omega_m\ln\left(\frac{144}{|\frac{1}{6}-E_{n+1}|}\right). \tag{29}$$

The right plot of Fig. 3 shows the phase space plot $(E-\frac{1}{6},\phi)$ of the whisker map for $B=0.003$ and $\omega_m=4$. The corresponding phase space map obtained from numerical solutions of the original dynamics equation [Eq. (17)] is shown in the left plot. Because particle orbits outside the separatrix for the original dynamical system are unbounded, the Poincaré map for those orbits has few points in the left plot. Within the stochastic layer of the whisker map, particles will eventually leak out to infinity.

Physics of the whisker map can be viewed as follows. For a given modulation tune ω_m, the condition for parametric resonances near the separatrix is determined approximately by Eq. (24). Because many $n{:}\ell$ parametric resonances overlap with one another near the separatrix, the stochasticity is localized mainly in the separatrix region. The width of stochastic layer, estimated from the linearized whisker map, is given by

$$\left|E-\frac{1}{6}\right|\leqslant\frac{3\pi\omega_m^4 B}{2\ \sinh\pi\omega_m}. \tag{30}$$

In reality, the width of the stochastic layer depends sensitively on ω_m due to occurrence of parametric resonances. For the QI dynamics system, the whisker map, which works mainly for the particle motion near separatrix orbits, may not be very useful in determining the stability criterion for the dynamical system.

In the presence of weak damping force, SFPs of parametric resonances turn into attractors. The right plot of Fig. 2 shows the basin of attraction corresponding to the SFPs with parameters $B=0.06$, $\omega_m=0.86$, and $A=0.05$ obtained from tracking 150×150 particles with an initial uniform distribution in the phase space. SFPs of dominant parametric resonances become attractors while SFPs of weak parametric resonances are destroyed. In general, the Hamiltonian in Eq. (21) is composed of a web of primary parametric resonances. The phase space locations of these resonance islands can be approximately obtained by drawing a horizontal line ω_m in Fig. 1. The location where the ω_m horizontal line intersects with the line $(n/\ell)Q(J)$, where n,ℓ are integers, is the phase space location where $n{:}\ell$ resonance occurs. As ω_m increases, it intersects only those parametric resonances with large n, where the strength function g_n is also small. Thus the stability of the dynamical system is less susceptible to high frequency perturbation. In the QI dynamical system, dominant parametric resonances are the $n=1$ and 2 modes. Since the strengths of the 1:1 and 2:1 parametric resonances are large, they can interact coherently to generate a series of secondary parametric resonances located in the range $\omega_m\in(1,2)$. These *overlapping* parametric resonances can be easily destroyed by the strong damping, however, they provide stochastic background for global chaos [1,11–13].

B. The 1:1 parametric resonance

When the damping parameter A of Eq. (17) becomes large, the attractor solutions or the periodic solutions can be obtained by harmonic linearization method [14]. The periodic solution of Eq. (17) for the 1:1 parametric resonance is given by

$$x=X_0+X_1\cos(\omega_m t+\chi_1).$$

Substituting the ansatz into Eq. (17) and keeping only the first harmonic in the expansion, we obtain

$$\omega_m^2 B^2=A^2\omega_m^2 X_1^2+(\omega_m^2-\sqrt{1-2X_1^2})^2 X_1^2, \tag{31}$$

with $\tan\chi_1=-\omega_m A/(\omega_m^2-\sqrt{1-2X_1^2})$, and $X_0=(1-\sqrt{1-2X_1^2})/2$. Figure 4 shows the amplitude X_1 of the periodic solution of Eq. (17) obtained numerically for $B=0.5$ with $A=0.1,0.3,0.5$, and 0.7, respectively. The solution of Eq. (31) for $B=0.5, A=0.7$ is also shown as a solid line. Figure 4 shows clearly that the periodic solution of the 1:1 parametric resonance plays a major role in particle motion in the QI Hamiltonian system at all modulation tunes except in the region of 2:1 parametric resonance.

From Eq. (31), we note that $X_1=1/\sqrt{2}$ represents the maximum oscillation amplitude for which this dynamical system is stable. Setting the maximum stable oscillation am-

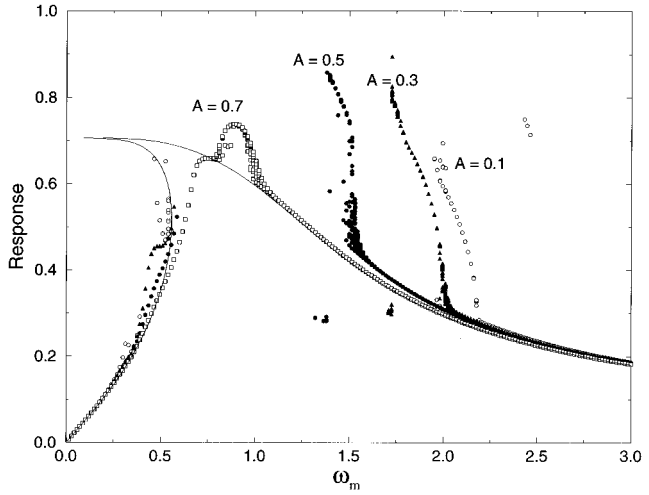

FIG. 4. The amplitude X_1 of the steady state solution, called response, obtained numerically is plotted as a function of ω_m for $B=0.5$ with damping parameter $A=0.1,0.3,0.5$, and 0.7, respectively. Solid lines correspond to the solutions of Eq. (31) for $A=0.7, B=0.5$. Two characteristic features shown in this figure are (1) the threshold tune of the 2:1 resonance decreases with increasing damping parameter A, and (2) the appearance of a very strong stop band around $\omega_m \approx 1$ for the 1:1 resonance.

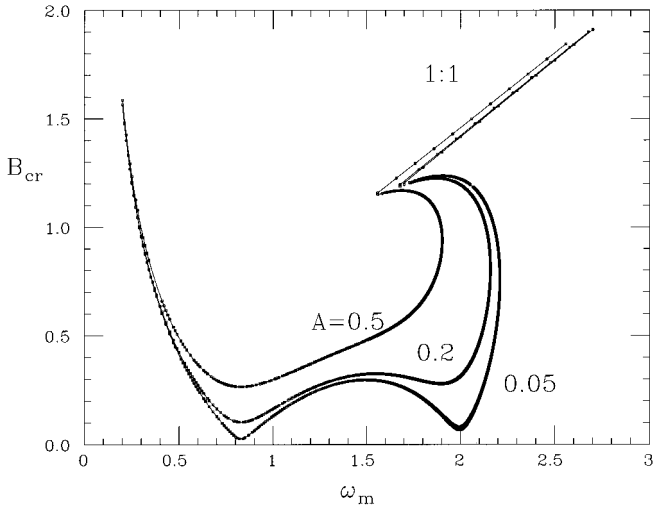

FIG. 5. The curves correspond to the threshold modulation amplitude $B_{2:1}$ for the 2:1 parametric resonance with damping parameter $A=0.05,0.2,0.5$, respectively. The critical modulation amplitude $B_{\mathrm{cr},1:1}$ for the 1:1 parametric resonance is also marked in the figure. The intercept of $B_{2:1}$ and $B_{\mathrm{cr},1:1}$, forming a cusp, corresponds to the bifurcation threshold of the 2:1 resonance on top of the limiting stable orbit for the 1:1 parametric resonance.

plitude as $X_1 = 1/\sqrt{2}$, the maximum tolerable modulation amplitude for the 1:1 parametric resonance is given by

$$B_{\mathrm{cr},1:1} = \frac{1}{\sqrt{2}}\sqrt{A^2+\omega_m^2} \tag{32}$$

for $\omega_m \geqslant 1$ [16]. At high modulation frequencies, the critical modulation amplitude for the 1:1 parametric resonance is a nearly linear function of the modulation frequency, i.e.,

$$B_{\mathrm{cr},1:1} \approx \frac{1}{\sqrt{2}}\omega_m .$$

C. The 2:1 parametric resonance

Next, our goal is to show that the 2:1 parametric resonance plays also an important role in chaos when the modulation tune lies in the region $\omega_m \leqslant 2$. First, we realize that when a friction term is added to the Hamiltonian system, the threshold 2:1 resonance tune is lowered, i.e., particles seemingly move slower in the phase space. This is evidently shown in Fig. 4, where the threshold modulation tune of the 2:1 parametric resonance is lowered as the damping parameter A increases. The reason that the threshold bifurcation tune of the 2:1 resonance is lowered will be addressed as follows.

The periodic solution associated with the 2:1 parametric resonance can be obtained by using the ansatz

$$x(t) = X_0 + X_1\cos(\omega_m t + \chi_1) + y(t). \tag{33}$$

The equation of motion for $y(t)$ is given by

$$y'' + Ay' + [1 - 2X_0 - 2X_1\cos(\omega_m t + \chi_1)]y \approx 0. \tag{34}$$

Let the solution of this damped Mathieu equation be

$$y(t) = X_{1/2}(s)\cos\left(\frac{\omega_m}{2}t + \chi_{1/2}\right). \tag{35}$$

The condition for the Mathieu instability can be obtained by assuming $X_{1/2} \sim e^{st}$ with $s \geqslant 0$, i.e.,

$$\left(\frac{\omega_m^2}{4} - \sqrt{1-2X_1^2}\right)^2 + A^2\frac{\omega_m^2}{4} \leqslant X_1^2. \tag{36}$$

The threshold of the Mathieu instability, corresponding to $s=0$, is obtained by setting equality to Eq. (36), where, for a given damping parameter A, the threshold amplitude X_1 can be expressed as a function of the modulation tune ω_m, and the threshold modulation amplitude $B_{2:1}$ can be obtained from Eq. (31). Figure 5 shows the $B_{2:1}$ vs ω_m for $A=0.05,0.2$, and 0.5 respectively. The curves in Fig. 5 represent the onset of the 2:1 parametric resonance. The dynamical system with parameters (B,ω_m) located on the line $B_{2:1}(\omega_m)$ encounters the threshold of the Mathieu instability.

Now we can understand the lowering of the threshold of ω_m vs A for the 2:1 parametric resonance shown in Fig. 4 as follows. When the damping parameter is increased, for a given B, the threshold tune of 2:1 parametric resonance, determined by Eqs. (31) and (36), is lowered due to a larger oscillation amplitude X_1 of the 1:1 parametric resonance. The corresponding $B_{\mathrm{cr},1:1}$ is also shown as lines marked 1:1 in Fig. 4. The entire bucket of the QI dynamics system disappears if parameters (B,ω_m) are above the $B_{\mathrm{cr},1:1}(\omega_m)$ line.

D. Stability of the dynamical system

The Melnikov integral method has often been applied to study the chaotic transition of many dynamical systems. If the stable and unstable orbits from a hyperbolic fixed point

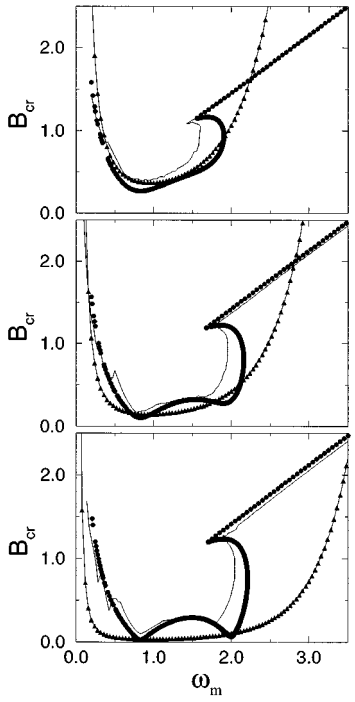

FIG. 6. The critical phase modulation amplitude $B_{\rm cr}$ (thin solid lines) obtained from numerical simulations is shown as a function of ω_m for $A=0.05$ (lower plot), $A=0.2$ (middle plot), and $A=0.5$ (top plot). The lines joining triangular symbols are $B_{\rm cr}$ obtained from the Melnikov integral method. Circle dots are $B_{\rm cr,1:1}$ and $B_{2:1}$ for the 1:1 and 2:1 parametric resonances. Note that the cusp in $B_{\rm cr}$ observed in numerical simulations is due to the transition from the 2:1 to the 1:1 parametric resonances.

cross each other, the dynamical system becomes homoclinic, which is an indicator of chaotic motion. The Melnikov integral for the QI system is given by [1]

$$D=\frac{6\pi\omega_m^3 B\sin\omega_m t_0}{\sinh\pi\omega_m}+\frac{6A}{5}, \tag{37}$$

where the condition for $D=0$ becomes

$$B_{\rm cr}=\frac{A}{5\pi}\frac{\sinh\pi\omega_m}{\omega_m^3}. \tag{38}$$

Based on the Melnikov integral method, the critical modulation amplitude $B_{\rm cr}$ for the chaotic condition is proportional to the damping parameter A.

Now we *define* the critical modulation amplitude $B_{\rm cr}$ as the minimum modulation amplitude such that the entire bucket is unstable. The thin solid line in Fig. 6 shows the critical modulation parameter $B_{\rm cr}$ as a function of ω_m obtained numerically with parameters $A=0.05$,0.2, and 0.5, respectively. The estimation obtained from the Melnikov integral is also shown as a line joining triangular symbols. Note that the Melnikov integral method fails in providing the A and ω_m dependence of the stability curve. The threshold $B_{2:1}$ of period-2 bifurcation and the critical modulation amplitude for the 1:1 parametric resonance, $B_{\rm cr,1:1}$, are also plotted as dots in the same figure. It is interesting to note that $B_{\rm cr}$ obtained from numerical simulation agrees in fine details

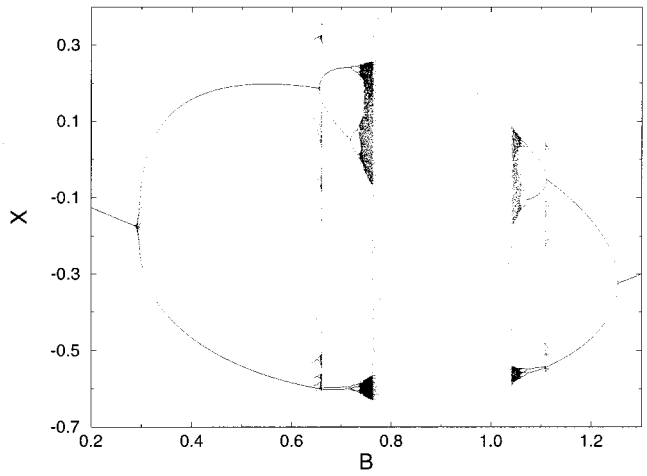

FIG. 7. The coordinate x of the Poincaré surface of section is plotted as a function of the modulation amplitude B at $\omega_m=1.975, A=0.2$. A sequence of period-2 bifurcations is observed leading to global chaos.

with the $B_{2:1}$ obtained from Eq. (36) for $0\leqslant\omega_m\leqslant 2$ and with $B_{\rm cr,1:1}$ for $\omega_m\geqslant 2$. This agreement indicates that the 2:1 parametric resonance plays an important role in the stability of the QI dynamical system. As an example, Fig. 9 in Ref. [1] shows that the QI dynamical system, when ω_m is varied, proceeds through a sequence of period-2 bifurcations in reaching global chaos with parameters $A=0.5, B=0.5$. In fact, the sequence of period-2 bifurcations will occur in the region of parametric space bounded by $B_{\rm cr}$ and $B_{2:1}$ curves shown in Fig. 6. This sequence of period-2 bifurcations appears in all possible parametric variations. For example, Fig. 7 shows attractor solutions of the QI dynamics system with $A=0.2, \omega_m=1.975$ as a function of the modulation amplitude B. This corresponds to drawing a vertical line in the middle plot of Fig. 6 with $\omega_m=1.975$. At $B\approx 0.3$, the dynamical system encounters Mathieu instability and undergoes period-2 bifurcation. The dynamical system evolves into global chaos via a sequence of period-2 bifurcations. When the vertical line intersects the thin solid line at $B\approx 0.75$, the system becomes completely unstable. As the modulation amplitude B is increased beyond 1.06, the dynamical system recovers from global instability and passes through a reversed sequence of period-2 bifurcation to reach a single steady state solution.

The evolution from disorder to order in the presence of a stronger modulation is due to the increase in the potential well depth created by the 1:1 parametric resonance. When the parameter B is larger than 1.35, the stable bucket area disappears, due entirely to the 1:1 parametric resonance. The parametric space bounded by the $B_{\rm cr}(\omega_m)$ line and the $B_{2:1}$ line in Fig. 6 will show the characteristics of period-2 bifurcation. Since the region of parametric space bounded by $B_{\rm cr}$ and $B_{2:1}$ is very small, the system becomes nearly unstable once the threshold of 2:1 parametric resonance is reached.

Figure 8 shows the attractor solution at $\omega_m=2.0$ (the upper plot) and $\omega_m=2.1$ (the lower plot) as a function of the modulation amplitude B with a damping parameter $A=0.2$. They correspond to two vertical lines at $\omega_m=2.0$ and 2.1

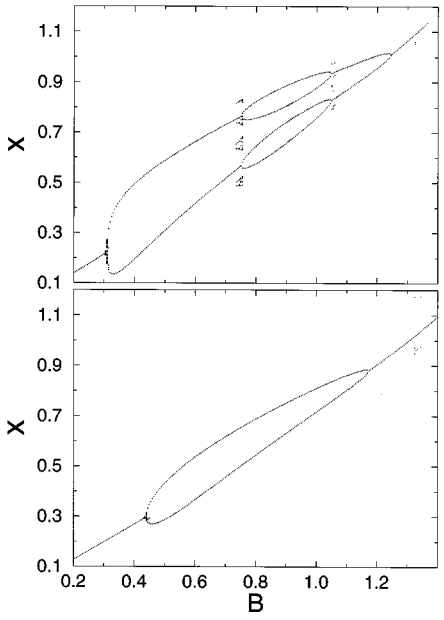

FIG. 8. The coordinate x of the Poincaré surface of section is plotted as a function of the modulation amplitude B at 2.0 (the upper plot) and $\omega_m = 2.1$ (the lower plot) with $A = 0.2$.

drawn in the middle plot of Fig. 6. Since these two lines do not intersect $B_{\rm cr}(\omega_m)$, the system does not reach global chaos, yet the sequence of period-2 bifurcations can be identified. In particular, the second period-2 bifurcation has to arise from the remnant time dependent term $\Delta H_{2:1}(t)$. Because the 2:1 parametric resonance has a finite width in the parametric space, it is evident that the course of global chaos would proceed through the sequence of period-2 bifurcations.

It is often misquoted in the literature that the instability of a dynamical system at a low modulation tune, e.g., $\omega_m \leqslant \frac{1}{2}$, proceeds through the Hopf bifurcation. We find from our numerical simulations that the above statement is not true for the QI dynamical system. At a small damping parameter A, the threshold of instability proceeds through subharmonic excitations due to the nonlinear term in the Hamiltonian, i.e., $B_{\rm cr} \leqslant B_{2:1}$ (see the bottom plot of Fig. 6). At a large damping parameter, the 2:1 parametric resonance becomes more important than the subharmonic terms, as shown in the top plot of Fig. 6, where $B_{2:1} \leqslant B_{\rm cr}$.

III. PARTICLE DYNAMICS IN QI WITH rf VOLTAGE MODULATION

In the presence of rf voltage modulation, the equation of motion for the normalized phase space coordinates is given by

$$p' = x - x^2, \tag{39}$$

$$x' = -p - bp\ \cos\omega_v t, \tag{40}$$

where the Hamiltonian is given by

$$H = H_0 + \frac{1}{2}p^2 b\ \cos\omega_v t. \tag{41}$$

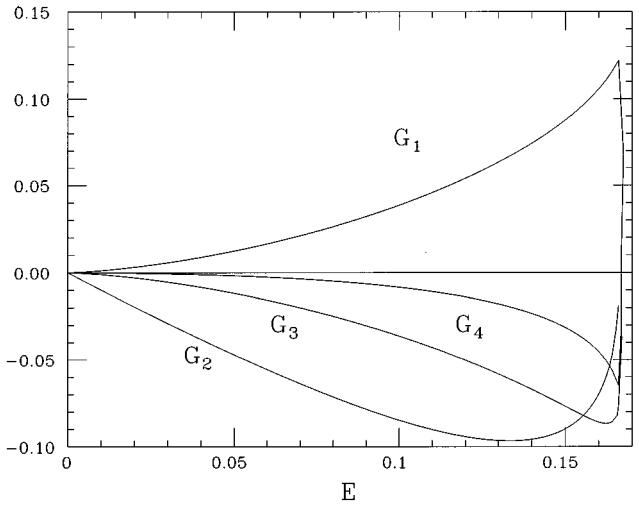

FIG. 9. The resonance strength functions G_n for $n = 1,2,3$, and 4 are plotted as a function of E. Note that $|G_2| > |G_1|$ in most regions of phase space. Thus the 2:1 parametric resonance is more important than the 1:1 parametric resonance for the voltage modulation.

Here H_0 is the unperturbed Hamiltonian of Eq. (5), and ω_v and b are modulation tune and the fractional modulation amplitude, i.e.,

$$\frac{\Delta V}{V} = b\ \cos\omega_v t.$$

A. Parametric resonances

When the voltage modulation amplitude b is small, the Hamiltonian can be expanded in action-angle variables (J,ψ) of the unperturbed Hamiltonian. Expanding p^2 in action-angle variables,

$$p^2 = \sum\ G_n e^{in\psi}, \tag{42}$$

where $G_{-n} = G_n^*$ the perturbed Hamiltonian of Eq. (41) becomes

$$H = H_0(J) + \frac{b}{4}\sum_{n=-\infty}^{\infty} G_n[e^{i(n\psi+\omega_v t)} + e^{i(n\psi-\omega_v t)}], \tag{43}$$

where $n = 0$ term does not affect particle motion, and the voltage modulation in the QI Hamiltonian contains all harmonics. Using Eq. (19), we find that the most important contribution in the voltage modulation comes from the $n = 2$ term, and all G_n vanishes at the separatrix orbit. The effect of the voltage modulation on particle motion is much weaker than the perturbation arising from the rf phase modulation (see Sec. III and Ref. [1]). Figure 9 shows G_n as a function of E for $n = 1,2,3$, and 4.

In general, the time dependent perturbation will not be important unless the stationary phase condition is satisfied. At the resonance condition

$$\omega_v \approx n\frac{d\psi}{dt} \approx nQ(J), \tag{44}$$

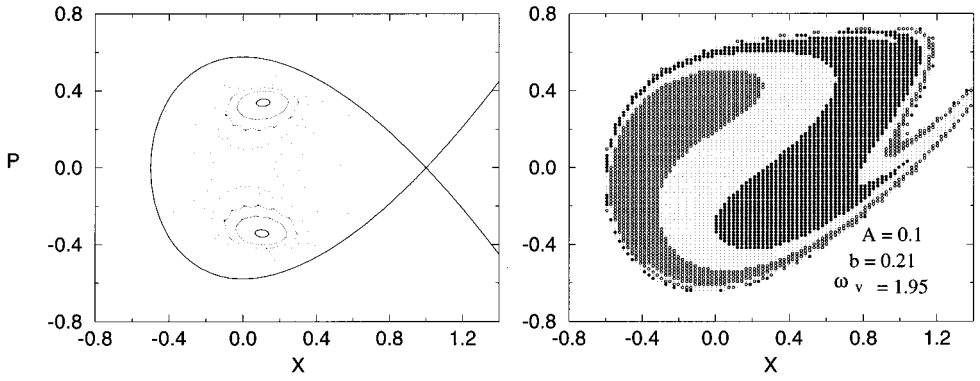

FIG. 10. The left plot shows the Poincaré surface of section for $A=0, b=0.21$, and $\omega_v=1.95$. Note that the stable region is limited to phase space region near the SFPs of 2:1 parametric resonance. The right plot shows the basin of attraction for $A=0.1, b=0.21$, and $\omega_v=1.95$. With a phase space damping, the stable phase space region is dramatically increased.

the stationary phase condition gives rise to coherent perturbation on Hamiltonian tori. Transforming the Hamiltonian into the resonance rotating frame with the generating function, $F_2=[\psi-(\omega_v/n)t]J_1$, the Hamiltonian is given by

$$H_{n:1}=H_0(J_1)-\frac{\omega_v}{n}J_1+\frac{1}{2}|G_n|\cos(n\psi_1+\chi_n)+\Delta H_{n:1}(t), \tag{45}$$

where we have lumped all incoherent terms into $\Delta H_{n:1}(t)$. The fixed points of the time averaged Hamiltonian are given by

$$\sin(n\psi_{1\mathrm{FP}}+\chi_n)=0, \quad \omega_v=nQ(J_{1\mathrm{FP}})\pm\frac{1}{2}n\left|\frac{dG_n}{dJ}\right|. \tag{46}$$

There are n SFPs and n UFPs for the resonance Hamiltonian. The perturbed Hamiltonian of Eq. (43) has generally a web of parametric resonances. When resonance islands overlap with one another, chaos can occur in the overlapping region of the phase space. The left plot of Fig. 10 shows the Poincaré surface of section for $\omega_v=1.95$ and $b=0.21$. Note here that stable motion is only localized near the SFPs of the 2:1 parametric resonance.

In the presence of phase space damping, the equation of motion becomes

$$p'=x-x^2, \tag{47}$$

$$x'=-p-bp\ \cos\omega_v t-Ax, \tag{48}$$

and the SFPs of parametric resonances become attractors. The right plot of Fig. 10 shows the basin of attraction with parameters $A=0.1, \omega_v=1.95$, and $b=0.21$. Here, the appearance of the center attractor in the right plot indicates that the tune of the dynamical system is slightly lowered, and the stable region in the phase space is also increased by the damping force.

B. Harmonic linearization method and periodic solutions

The Hamiltonian formalism is not applicable when the damping parameter A of Eq. (17) becomes large. The attractor solutions or the periodic solutions can be obtained by harmonic linearization method [14]. Let the ansatz of Eqs. (47) and (48) be given by

$$x=X_0+X_1\cos(\omega_v t+\chi_1), \tag{49}$$

$$p=P_0+\frac{X_1\sqrt{1-2X_1^2}}{\omega_v}\sin(\omega_v t+\chi_1). \tag{50}$$

Substituting the ansatz into Eqs. (48), we obtain

$$\begin{aligned}&[A^2\omega_v^2+(\omega_v^2-\sqrt{1-2X_1^2})^2\\&\quad+b^2\sqrt{1-2X_1^2}(\omega_v^2-\sqrt{1-2X_1^2})]X_1\\&=-\frac{b}{2}\omega_v A(1-\sqrt{1-2X_1^2})\\&\quad\times\sqrt{A^2\omega_v^2+(\omega_v^2-\sqrt{1-2X_1^2})^2},\end{aligned} \tag{51}$$

with $\tan\chi_1=(\omega_v^2-\sqrt{1-2X_1^2})/(-\omega_v A)$ and $X_0=(1-\sqrt{1-2X_1^2})/2$. In the weak damping and small modulation amplitude approximation, the modulation amplitude is related to modulation tune by $\omega_v\approx 1-\frac{1}{2}X_1^2$, which agrees reasonably well with that of Eq. (51) for the $n=1$ mode. The amplitude of attractors obtained from numerical simulations is shown in Fig. 11 for $A=0.01$ and $B=0.3$. Solid lines show the solution of Eq. (51) for the 1:1 resonance. Other attractor solutions can be identified as 2:1, 3:1, 3:2, and 5:2 parametric resonances.

Note that $X_1=0$ is a solution of Eq. (51) for all ω_v. However, Fig. 11 shows that there is a gap of $\omega_v\approx 2$, where $X_1=0$ is not a solution of Eq. (51). This gap of $\omega_v=2$ corresponds to the Mathieu instability. The steady state solution at $\omega_v\approx 2$ can be obtained by the ansatz

$$x(t)=X_0+X_1\cos(\omega_v t+\chi_1)+y(t), \tag{52}$$

where $y(t)$ satisfies

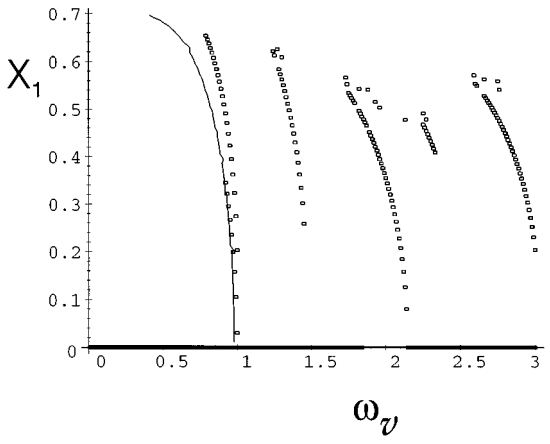

FIG. 11. The amplitudes of periodic solutions are shown as a function of the voltage modulation tune ω_v for $A=0.01$ and $b=0.3$. Note that 1:1, 3:2, 2:1, 5:2, 3:1 resonances are excited due to a very weak damping parameter $A=0.01$.

$$y''+\left(A+\frac{b\omega_v}{1+b\ \cos\omega_v t}\right)y'+\left[1-2(1+b\ \cos\omega_v t)\times[X_0+X_1\cos(\omega_v t+\chi_1)]+\frac{b\omega_v A}{1+b\ \cos\omega_v t}\right]y=0. \tag{53}$$

This is the generalized Mathieu equation with phase space damping. The general solution can be expressed as

$$y=X_{1/2}\cos\left(\frac{\omega_v}{2}t+\chi_{1/2}\right). \tag{54}$$

In a finite tune window, the amplitude has a solution $X_{1/2}\sim e^{st}$ with $s>0$. Thus $X_{1/2}=0$ corresponds to the UFP of 2:1 parametric resonance in Eq. (46). This instability is called the Mathieu instability.

C. Transition to global chaos and Melnikov integral

We observe in the previous few sections that the QI dynamics system will encounter global chaos when the modulation amplitude is large. What is the critical modulation amplitude for the onset of global chaos? Using (47) and Eqs. (48), the distance between the stable and unstable orbits from the UFP of the unperturbed Hamiltonian is given by the Melnikov integral [14]

$$D=\int_{\infty}^{\infty}[x_{sx}(t)-x_{sx}^2(t)][bp_{sx}(t)\cos\omega_v(t+t_0)+Ap_{sx}(t)]dt$$
$$=\frac{3}{4}\pi b\omega_v^2(\omega_v^2+1)(1-\omega_v^2)\sin\omega_v t_0\,\mathrm{csch}(\pi\omega_v)+\frac{6A}{5}, \tag{55}$$

where x_{sx} and p_{sx} of the separatrix orbit given by Eq. (9) have been used to obtain the Melnikov integral. The condition for a homoclinic structure near the separatrix is given by

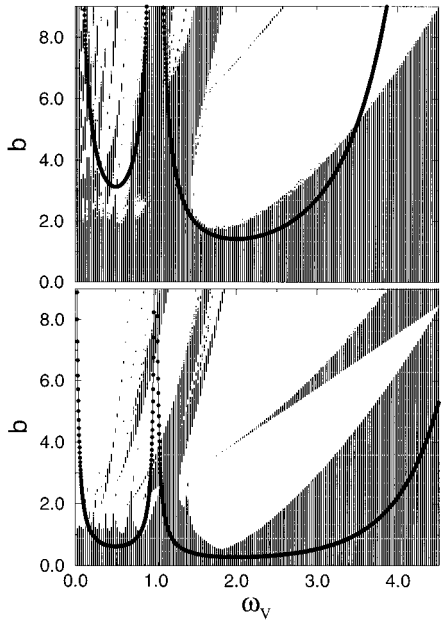

FIG. 12. The shaded areas mark the stable regions of the QI dynamical system under the rf voltage modulation with the damping parameter $A=0.1$ (lower plot), and $A=0.5$ (upper plot), respectively. The white areas in (b,ω_v) correspond to the condition that the entire bucket is unstable. For completeness, we include the parametric region $b>1$ in our study of the stability of the QI dynamical system. The solid line that connects dots corresponds to the critical modulation amplitude obtained from the Melnikov integral method.

$$b_{\mathrm{cr}}=\frac{2A\ \sinh\pi\omega_v}{\pi\omega_v^2(\omega_v^2+1)|\omega_v^2-1|}. \tag{56}$$

Based on the Melnikov integral method, the critical modulation amplitude b_{cr} for the chaotic condition is proportional to the damping parameter A. Note also that the Melnikov integral has a pole at $\omega_v=1$. This means that the $n=1$ harmonic is usually not excited by the rf voltage modulation. The physics is that the rf voltage modulation at a tune of $\omega_v=1$ can be averaged to zero, and the particle motion can tolerate a large voltage modulation amplitude. In reality, the dynamical system with amplitude modulation is complicated because many subharmonics can be excited by the Mathieu instability.

To provide a complete analysis on the stability of the QI dynamical system under rf voltage modulation, we perform extensive numerical simulations, where the critical modulation amplitude is *defined* as the condition that the entire bucket is unstable. The shaded areas of Fig. 12 depict parametric regions (b,ω_v) where there exist stable phase space points in the bucket. In other words, parameters in the white space regions correspond to the result that the entire rf bucket is unstable. The critical modulation parameter b_{cr} for the onset of global chaos can be identified as the boundary between the shaded area and the white space. Although $b>1$ is unphysical, the stability of this dynamical system is studied in the entire parametric space for completeness. The estimation obtained from the Melnikov integral is also shown for comparison. We observe that the Melnikov integral does not provide detailed understanding of the stability of this dynamical system.

IV. CONCLUSION

In conclusion, we have identified the role of parametric resonances in the transition to global chaos for the QI dynamical system. At $\omega_m \geqslant 2$, the stability of the dynamical system is determined mainly by the 1:1 parametric resonance. At $\omega_m \approx 2$, the 2:1 parametric resonance, on top of the 1:1 parametric resonance, causes the SFP of the 1:1 resonance to be unstable (Mathieu instability). This gives rise to a global instability to the entire QI bucket. Thus the characteristics of global chaos (instability) for $\omega_m \leqslant 2$ will proceed through a sequence of period-2 bifurcation, which arises from the 2:1 parametric resonance. For the QI dynamical system, the stability can be obtained reliably by the method of parametric resonance analysis, while the Melnikov integral method fails even to provide a proper dependence of the stability on the modulation tune and the damping parameter. We have also studied the effect of voltage modulation on the QI dynamical system. We find that the QI dynamical system is insensitive to rf voltage modulation provided that the voltage modulation amplitude b is smaller than 0.2.

ACKNOWLEDGMENTS

Work supported in part by the DOE, Grant No. DOE-DE-FG02-93ER40801 and NSF, Grant No. PHY-9512832.

[1] A. Riabko, Phys. Rev. E **54**, 815 (1996).
[2] C. Pelligrini and D. Robin, Nucl. Instrum. Methods A **301**, 27 (1991).
[3] D. Robin, E. Forest, C. Pelligrini, and A. Amiry, Phys. Rev. E **48**, 2149 (1993); H. Bruck *et al.*, IEEE Trans. Nucl. Sci. **NS20**, 822 (1973).
[4] L. Liu *et al.*, Nucl. Instum. Methods A **329**, 9 (1993).
[5] H. Hama, S. Takano, and B. Isoyoma, Nucl. Instrum. Methods A **329**, 29 (1993); S. Takano, H. Hama, and G. Isoyama, Jpn. J. Appl. Phys. **32**, 1285 (1993).
[6] A. Nadji, in *Proceedings of the 4th European Particle Accelerator Conference*, edited by V. Suller and Petit-Jean-Genas Christine (World Scientific, Singapore, 1994), p. 128.
[7] D. Robin, H. Hama, and A. Nadji, Lawrence Berkeley Report No. LBL-37758, 1995 (unpublished).
[8] D. Robin *et al.*, SLAC Report No. SLAC-PUB-95-7015, 1995 (unpublished).
[9] D. F. Lawden, in *Elliptic Functions and Applications*, Applied Mathematical Sciences Vol. 80 (Springer-Verlag, New York, 1989).
[10] *Handbook of Mathematical Functions*, edited by M. Abramowitz and I. A. Stegun (National Bureau of Standards, Washington, DC, 1975).
[11] S. Y. Lee *et al.*, Phys. Rev. E **49**, 5717 (1994); J. Y. Liu *et al.*, *ibid.* **50**, R3349 (1994); J. Y. Liu *et al.*, Part. Accel. **49**, 221 (1995).
[12] D. Li *et al.*, Phys. Rev. E **48**, R1638 (1993); Nucl. Instrum. Methods A **364**, 205 (1995).
[13] H. Huang *et al.*, Phys. Rev. E **48**, 4678 (1993); M. Ellison *et al.*, Phys. Rev. Lett. **70**, 591 (1993); M. Syphers *et al.*, *ibid.* **71**, 719 (1993); Y. Wang *et al.*, Phys. Rev. E **49**, 1610 (1994).
[14] T. Kapitaniak, *Chaotic Oscillations in Mechanical Systems* (Manchester University Press, Manchester, 1991).
[15] B. V. Chirikov, Phys. Rep. **52**, 263 (1979).
[16] For $\omega_m \leqslant 1$, there may exist two SFPs for the 1:1 parametric resonance. The stability condition of the inner attractor is not given by Eq. (32).